

How limit cycles and quasi-cycles are related in systems with intrinsic noise

Richard P. Boland,^{*} Tobias Galla,[†] and Alan J. McKane[‡]
*Theoretical Physics Group, School of Physics and Astronomy,
 University of Manchester, Manchester M13 9PL, United Kingdom*
 (Dated: November 1, 2018)

Fluctuations and noise may alter the behavior of dynamical systems considerably. For example, oscillations may be sustained by demographic fluctuations in biological systems where a stable fixed point is found in the absence of noise. We here extend the theoretical analysis of such stochastic effects to models which have a limit cycle for some range of the model parameters. We formulate a description of fluctuations about the periodic orbit which allows the relation between the stochastic oscillations in the fixed point phase and the oscillations in the limit cycle phase to be elucidated. In the case of the limit cycle, a suitable transformation into a co-moving frame allow fluctuations transverse and longitudinal with respect to the limit cycle to be effectively decoupled. While longitudinal fluctuations are of a diffusive nature, those in the transverse direction follow a stochastic path more akin to an Ornstein-Uhlenbeck process. Their power spectrum is computed analytically within a van Kampen expansion in the inverse system size. This is carried out in two different ways, and the subsequent comparison with numerical simulations illustrates the effects that can occur due to diffusion in the longitudinal direction.

PACS numbers: 05.40.-a, 02.50.Ey, 82.40.Bj

I. INTRODUCTION

The effect of noise on nonlinear dynamical systems has been studied for some time [1] and is now a substantial field, yet significant new aspects continue to be unearthed. One of the most recent of these concerns systems which fundamentally involve discrete entities, for example individuals in an ecological system. These have populations which are modeled stochastically, for example random births and deaths. In such cases it may be that stochastic effects alter the behavior of non-linear systems substantially, and crucial differences between the properties of a given system can be observed in the presence and in the absence of noise. Examples can be found in the context of predator-prey population dynamics [2, 3], in evolutionary game theory [4, 5], in cyclic trapping reactions [6], in models of opinion dynamics [7], in epidemics [8, 9, 10] and in connection with genetic networks [11] or biochemical clocks [12, 13]. In these cases the “noise” is intrinsic to the system itself; in the parlance of ecology it is ‘demographic stochasticity’, rather than environmental stochasticity.

One of the most intriguing effects found in these systems concerns the existence of oscillatory behavior. It has long been conjectured that in some situations the influence of noise due to demographic stochasticity would be sufficient to perturb the stationary state, predicted by a deterministic or mean-field type analysis, to produce cyclic behavior [14]. Oscillatory behaviors of this kind are referred to as

quasi-cycles [15]. This effect can be demonstrated in a simple and straightforward way, and analytic results derived show very good agreement with simulations [2]. This latter study conclusively demonstrates that while the deterministic limits of models of these systems exhibit stable fixed-point behavior, their stochastic analogues show resonant and persistent oscillations about these fixed point solutions.

The starting point for formulating models of this kind is to define the system with a *finite* number of constituents (e.g. molecules in a chemical reaction system, individuals in the context of population dynamics, or agents in models of social dynamics) which interact according to a given set of possible reactions, whose occurrence is determined by random factors (see e.g. [16, 17] and references therein). In spatial diffusive systems, for example, a certain molecular reaction may occur only if all necessary reactants are present at a given site in space and time, and similarly a predator in a model of population dynamics may feed upon a unit of prey, only if both meet. Events such as birth and death typically occur at random with Poisson statistics in such systems, providing another source of stochasticity [17]. This is demographic stochasticity. In the limit of infinite particle numbers, such systems are faithfully described by deterministic equations, also called rate equations. These ordinary differential equations for concentrations of the different reactants address the behavior of the system on a mean-field level. Assuming a well-mixed population the rate equations are zero-dimensional and describe uniform densities as functions of time. The stochasticity present on the level of interactions between individuals is averaged out in this case of an infinite system size. On the other hand, a systematic study of first-order corrections to the rate equations due to finite system

^{*}Electronic address: richard.p.boland@postgrad.man.ac.uk

[†]Electronic address: tobias.galla@manchester.ac.uk

[‡]Electronic address: alan.mckane@manchester.ac.uk

size can be made. Such studies have captured the behavior of fluctuations about the stationary mean-field solution which are small enough that a linear approximation is sufficient. In several examples, the power spectra of the fluctuations have been computed analytically [2, 8, 13].

The aim of the present paper is to extend these existing analytical descriptions of finite-size stochastic effects to systems which on the mean-field level do not always approach a stable fixed point, but instead may tend towards a stable and periodic limit cycle solution for some range of the parameters. The effects of demographic stochasticity on such systems have been studied numerically, for example in [3] for predator-prey systems with a non-linear functional response. There the shape of the resulting autocorrelation functions of predator or prey densities have been used to help to distinguish between noisy limit cycles and quasi-cycles. This problem could equivalently be analyzed by looking at the power spectra. Distinguishing these two types of cyclic motion might also be of relevance in the context of biochemical clocks [12] and genetic networks [11]. Also of interest is to understand what happens at the boundary between the regimes where there is a stable fixed point and where there is a stable limit cycle. Do the cycles continuously merge with each other or are they unrelated?

To develop the analytical tools required to study such systems, we focus on the Brusselator model [11, 16, 18, 19, 20, 21, 22]. This model is a simple example of an auto-catalytic, oscillating chemical reaction [18, 23]. Auto-catalytic reactions are those in which the presence of a given reactant acts to increase the rate of its own production. A real-world realization of oscillatory chemical reactions is given by the celebrated Belousov-Zhabotinsky reaction [24]. The corresponding deterministic rate equations are known to have limit cycle solutions provided that model parameters (i.e. reaction rates) are suitably chosen [16, 21]. It also has the properties required to show resonant oscillations in the regime where a stable fixed point exists. Therefore it has the necessary features required for our investigation.

Earlier studies of the Brusselator system, e.g. by Tomita et al. [22] or by Scott et al. [11] have addressed finite-size corrections to the dynamics of this system based on van Kampen expansions of the corresponding master equation [25], but to the best of our knowledge no systematic attempts have been made to study temporal correlations (i.e. autocorrelation functions or power spectra) of this system. Specifically, our objective is to build on the calculations performed in [22], and in particular to address these temporal correlations analytically. We also present a systematic account of different schemes of transformation into a co-moving frame (following the motion of the deterministic system around the limit cy-

cle). We link these with different interpretations of stochastic simulations based on the Gillespie algorithm [26]. It should be noted that recent studies by Frey et al. [4, 5] also address models with limit cycles but those expansions are performed about unstable fixed points in the interior of the limit cycle, whereas an expansion about the cycle itself is carried out in the present work.

The remainder of the paper is organized along the following lines. In section II, we introduce the model system initially as a mean field model and later as an individual based model. We then introduce the techniques of the van Kampen system-size expansion in Section III by applying them to the case where the mean-field dynamics approach a fixed point. A linearization about a stable limit cycle solution is carried out in Section IV; we describe the limit cycle itself, the analysis of the Floquet multipliers and exponents and finally we discuss the co-moving Frenet frame. In Section V we use these tools to study the full stochastic problem of large but finite systems containing a limit cycle in the mean field. We derive the power spectrum describing the fluctuations in this case and also compare this prediction against numerical simulations of the individual-based Brusselator model under two different possible interpretations. In the final section we summarize our results and provide an outlook for future work.

II. THE BRUSSELATOR MODEL

A. Deterministic mean-field rate equations

The non-spatial Brusselator model is well known in the form of the mass-action kinetic equations in two dynamic variables $x_1(t) \geq 0$ and $x_2(t) \geq 0$ representing the time-dependent concentrations of a pair of dynamic reagents. These equations are of the form [16, 21, 22]

$$\begin{aligned}\dot{x}_1 &= 1 - x_1(1 + b - cx_1x_2), \\ \dot{x}_2 &= x_1(b - cx_1x_2),\end{aligned}\tag{1}$$

where b and c are constant and positive model parameters related to the reaction rates. Since they will form the basis of the work we will describe in this paper, we will briefly review the structure of these equations. Further details may be found in textbooks on nonlinear dynamics, for instance [21]. For simplicity we will use the shorthand $\mathbf{x}(t) = (x_1(t), x_2(t))$ for the two-dimensional vector of concentrations.

The two-dimensional and first-order nature of the Brusselator restricts the class of solutions to three possibilities. We may have fixed points at which the left-hand side of Eq. (1) vanishes, limit cycles where the dynamics repeats in a periodic orbit or a unbounded behavior where the solution tends towards infinity and never returns. It turns out that

this last possibility can be eliminated for the Brusselator if we require that the dynamics begins within the positive quadrant ($x_1 > 0$ and $x_2 > 0$) and also that we have positive and finite parameter values. A limit cycle does exist for a range of parameter values; this will be discussed in Section IV A. This leaves fixed points, which we will discuss here. It turns out that there is only one fixed point of Eq. (1) given by $\mathbf{x}^* = (x_1^*, x_2^*) = (1, (b/c))$. The behavior of the system close to this fixed point can be understood within a linear stability analysis. To this end, one considers a deviation $\varepsilon \boldsymbol{\xi}(t) \equiv \mathbf{x}(t) - \mathbf{x}^*$ from the fixed point. The pre-factor ε here indicates that we assume these deviations to be small. Later, in the context of a van Kampen expansion, this parameter will take on a specific meaning in terms of the system size. Assuming that an expansion to linear order is appropriate, one then has

$$\dot{\boldsymbol{\xi}} = K^* \boldsymbol{\xi}, \quad (2)$$

where the Jacobian at the fixed point is given by

$$K^* = \begin{pmatrix} b-1 & c \\ -b & -c \end{pmatrix}. \quad (3)$$

The eigenvalues of the matrix K^* determine the stability or otherwise of the fixed point (x_1^*, x_2^*) . They are both found to be real so long as $|b-1-c| > 2\sqrt{c}$. Otherwise the eigenvalues form a complex conjugate pair with a real part which is negative if $b < 1+c$. The line $b = 1+c$ is a family of Hopf bifurcations which separate the parameter space into two phases: one in which there exists a single globally stable fixed point ($b < 1+c$) and another in which there is a single globally stable limit cycle ($b > 1+c$). The resulting phase diagram is depicted in Fig. 1.

B. Microscopic multi-particle dynamics

We can also discuss the Brusselator on the level of individual molecules. In this case, the system is described by four chemical reactions between four substances, A, B, X_1 and X_2 [16, 21, 22]. The number of A and B particles is, by construction, constant in time, so that their populations do not form degrees of freedom; their role is merely to set the reaction rates. The state of the system at any time is therefore described by the number of molecules of each of the two substances X_1 and X_2 , denoted by $n_1(t)$ and $n_2(t)$. Both of these are non-negative integers at any time and we will define $\mathbf{n} = (n_1, n_2)$. The molecules are considered to interact randomly due to short-timescale fluctuations such as thermal activation. Hence we model their occurrence with Poisson statistics. As such we need only specify the expected number of occurrences per unit time for each reaction. We denote these transition rates as T_ν for

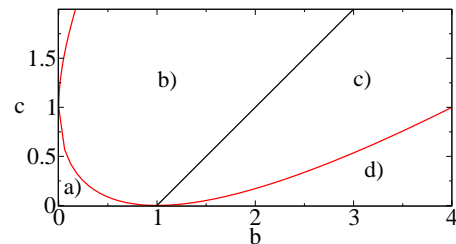
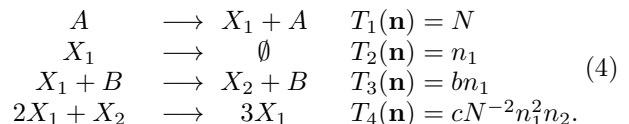


FIG. 1: (Color on-line) Phase diagram of the Brusselator fixed point at $\mathbf{x}^* = (1, (b/c))$ as obtained from the deterministic (mean-field) theory, Eq. (1). Behavior in the different regions is as follows: a) stable, non-oscillatory (both eigenvalues real and negative), b) stable, oscillatory (eigenvalues complex, negative real part), c) unstable, oscillatory (eigenvalues complex, positive real part), d) unstable, non-oscillatory (both eigenvalues real and positive). Note that there is a stable limit cycle in both c) and d).

$\nu \in \{1, \dots, 4\}$, which are in turn functions of the population vector \mathbf{n} . The reactions of the Brusselator are given here alongside their corresponding transition rate,



Note that different microscopic formulations of the Brusselator can be found in the literature (see e.g. [26, 27, 28]), with their differences pertaining only to the precise role of the non-dynamical substances. We here follow the formulation of [22].

The rates, $T_\nu(\mathbf{n})$, are derived according to the stoichiometric weights of each type of molecule on the left-hand side of each reaction. The first reaction effectively corresponds to the (spontaneous) creation of X_1 molecules. The rate of this reaction is proportional to the number of A molecules which we parametrize by the integer N and hence we use $T_1(\mathbf{n}) = N$. The spontaneous decay of X_1 molecules, $X_1 \rightarrow \emptyset$, occurs with a rate proportional to n_1 and will be set to $T_2(\mathbf{n}) = n_1$. There is no loss of generality by doing this since we can consider this reaction as setting the time scale of the model. With the choices made so far, the first two reactions in isolation ensure that the mean number of X_1 molecules over time is N (see for example [17]). The third reaction converts molecules of type X_1 into type X_2 and occurs at rate $T_3(\mathbf{n}) = bn_1$, where b is a parameter equal to the ratio of the number of B molecules to that of A molecules. The fourth reaction is of an auto-catalytic nature (with X_1 being both a reactant and a product of the reaction) and will convert X_2 into X_1 at a rate

which is quadratic in n_1 and linear in n_2 . More precisely, the rate of this fourth reaction is proportional to $n_1(n_1 - 1)$. However, we shall assume that $n_1 \gg 1$ at all times and that $T_4(\mathbf{n})$ is well approximated by $T_4(\mathbf{n}) = cN^{-2}n_1^2n_2$. The factor of N^{-2} ensures that c is of the same dimension as the parameter b . So long as b and c are independent of N , n_2 also scales with N and hence N controls the total number of particles in the system. This justifies the use of the label *system size* for the parameter N .

The stochastic time evolution of the system can be described by a master equation. To compactify notation we will encode the effect of an occurrence of reaction $\nu \in \{1, \dots, 4\}$ on the system in a vector \mathbf{v}_ν describing the change of populations due to this reaction. The first component of \mathbf{v}_ν denotes the change in the number of X_1 molecules due to the single occurrence of reaction ν , and the second component the change in the number of X_2 molecules. For example, an occurrence of the first reaction increases n_1 by one while leaving n_2 unchanged. In all we have,

$$\begin{aligned} \mathbf{v}_1 &= (1, 0), & \mathbf{v}_2 &= (-1, 0), \\ \mathbf{v}_3 &= (-1, 1), & \mathbf{v}_4 &= (1, -1). \end{aligned} \quad (5)$$

The evolution of the time-dependent probability, $P_{\mathbf{n}}(t)$, of finding the system in state $\mathbf{n} = (n_1, n_2)$ at time t is described by the master equation,

$$\frac{d}{dt}P_{\mathbf{n}}(t) = \sum_{\nu=1}^4 (T_\nu(\mathbf{n} - \mathbf{v}_\nu)P_{\mathbf{n}-\mathbf{v}_\nu}(t) - T_\nu(\mathbf{n})P_{\mathbf{n}}(t)), \quad (6)$$

subject to initial conditions $P_{\mathbf{n}}(t_0)$. The first term in the summation accounts for transitions of the system state from $\mathbf{n} - \mathbf{v}_\nu \rightarrow \mathbf{n}$ while the second term accounts for transitions away from the state \mathbf{n} .

While the problem of solving the master equation exactly is intractable, the mean-field behavior of the system, Eq. (1), may be recovered by multiplying the master equation on both sides by the population vector \mathbf{n} followed by a summation over all possible configuration states. This leads to

$$\frac{d}{dt}\langle \mathbf{n} \rangle = \sum_{\nu=1}^4 \mathbf{v}_\nu \langle T_\nu(\mathbf{n}) \rangle, \quad (7)$$

where the brackets $\langle \dots \rangle$ denote a time-dependent ensemble average over realizations of the stochastic dynamics, i.e. $\langle f(\mathbf{n}) \rangle = \sum_{\mathbf{n}} P_{\mathbf{n}}(t)f(\mathbf{n})$ for any function $f(\mathbf{n})$ of the state-vector. We shall now also use the mean-field approximation $\langle T_\nu(\mathbf{n}) \rangle \approx T_\nu(\langle \mathbf{n} \rangle)$, which amounts to neglecting correlations by replacing $\langle n_1^2 n_2 \rangle$ with $\langle n_1 \rangle^2 \langle n_2 \rangle$. To simplify notation further we define the dimensionless variable $\mathbf{x}(t) \equiv N^{-1} \langle \mathbf{n}(t) \rangle$ and dimensionless transition rates $a_\nu(\mathbf{x})$ through the identity $Na_\nu(\mathbf{x}) \equiv T_\nu(N\mathbf{x})$ for all reactions. Finally, the rate of change of the mean-field

concentration is

$$\dot{\mathbf{x}} = \mathbf{A}(\mathbf{x}) = \sum_{\nu} \mathbf{v}_\nu a_\nu(\mathbf{x}), \quad (8)$$

where ν runs over all reactions. In the Brusselator we have

$$\begin{aligned} a_1(\mathbf{x}) &= 1, & a_2(\mathbf{x}) &= x_1, \\ a_3(\mathbf{x}) &= bx_1, & a_4(\mathbf{x}) &= cx_1^2x_2, \end{aligned} \quad (9)$$

and so we have the functions $A_1(\mathbf{x}) = 1 - x_1(1 + b - cx_1x_2)$ and $A_2(\mathbf{x}) = x_1(b - cx_1x_2)$ which agrees with the right-hand sides of the mass-action equations (see Eq. (1)). We shall see that the definition of $a_\nu(\mathbf{x})$ finds further use in the following section.

III. STOCHASTIC EFFECTS IN THE FIXED-POINT PHASE

One of the aims of this paper is to understand how the cycles generated by stochastic amplification, in the regime where a stable fixed point exists, behave as parameters change so that the fixed point becomes unstable and a limit cycle is born. Therefore in this section we examine the nature of these stochastic cycles by restricting the analysis to choices of the model parameters corresponding to points in phase b) of Fig. 1.

In the previous section we showed that the average dynamics of a large ensemble of the finite Brusselator system, defined by the reaction dynamics of Eq. (4), will follow the deterministic path laid out by Eq. (1). Individual realizations will, of course, follow random paths but simulations show these will move towards and subsequently stay close to the fixed point. In particular the random fluctuations away from a stable fixed point solution are of relative order $1/\sqrt{N}$, as has been observed in similar analysis of other reaction systems [2, 8, 13, 22]. The characteristics of the fluctuations can be studied analytically by means of an expansion of the master equation in the inverse system size [25]. This is a standard tool in the analysis of interacting particle systems, commonly referred to as van Kampen's system-size expansion, which has been applied to a number of different systems e.g. in [2, 8, 13, 22], so we will not present the full details of the mathematical analysis here. Some of the intermediate steps are reported in the Appendix. The key idea is to write the particle populations n_1 and n_2 of the finite system as

$$\begin{aligned} n_1/N &= x_1^* + \xi_1/\sqrt{N}, \\ n_2/N &= x_2^* + \xi_2/\sqrt{N}. \end{aligned} \quad (10)$$

It follows that ξ_1 and ξ_2 are also random variables which represent the fluctuations of the dynamics of the finite system about the stationary solution of

the mean-field equations. We will frequently use the shorthand $\xi = (\xi_1, \xi_2)$. A systematic expansion of the master equation (6) in powers of $N^{-1/2}$ is then carried out following the lines of [25]. The leading order terms yield the deterministic mean-field equations while the next-to-leading order terms give rise to a linear Fokker-Planck equation (see Eq. (A-8)), describing the time evolution of the probability density function of ξ . The corresponding drift matrix is the Jacobian K^* of the deterministic dynamics (as defined in Eq. (3)). The appearance of K^* should not be surprising: Eq. (10) has the same form used in the linear stability analysis of Section II A, with $\epsilon = 1/\sqrt{N}$. The diffusion matrix, D^* , in the Fokker-Planck equation is given by Eq. (A-10) evaluated at the fixed point. This yields,

$$D^* = \begin{pmatrix} (1+b) & -b \\ -b & b \end{pmatrix}. \quad (11)$$

The Fokker-Planck equation (A-8) is equivalent to a Langevin system of the form

$$\dot{\xi}(t) = K^* \xi(t) + \mathbf{f}(t), \quad (12)$$

where $\mathbf{f}(t) = (f_1(t), f_2(t))$ is bivariate Gaussian white noise of zero mean and with the following co-variance matrix indicating correlations between components:

$$\langle f_i(t) f_j(t') \rangle = 2D_{ij}^* \delta(t - t') \quad i, j \in \{1, 2\}. \quad (13)$$

Due to the linear character of Eq. (12) and given that the drift matrix is constant in time it is straightforward to obtain analytical expressions for the power spectra $P_1(\omega) = \langle |\tilde{\xi}_1(\omega)|^2 \rangle$ and $P_2(\omega) = \langle |\tilde{\xi}_2(\omega)|^2 \rangle$. We have here written $\tilde{\xi}_i(\omega)$ for the Fourier transform of the fluctuating variables $\xi_i(t)$ ($i = 1, 2$) with,

$$\tilde{\xi}_i(\omega) = \int_{-\infty}^{\infty} \xi_i(t) e^{-i\omega t} dt. \quad (14)$$

Following the steps of [2, 8, 13] one finds

$$P_1(\omega) = 2((1+b)\omega^2 + c^2) \mathcal{D}^{-1}(\omega), \quad (15)$$

$$P_2(\omega) = 2b(\omega^2 + 1 + b) \mathcal{D}^{-1}(\omega), \quad (16)$$

$$\mathcal{D}(\omega) = (c - \omega^2)^2 + (1 + c - b)^2 \omega^2. \quad (17)$$

As seen in Fig. 2 these spectra each show a maximum at a non-zero frequency, indicating amplified coherent oscillations due to the demographic noise. These analytical predictions compare well against simulations for different values of the model parameters b and c well inside the fixed-point phase. Numerical estimates for the power spectra are obtained through the repeated simulation of the microscopic chemical reactions using the Gillespie algorithm [26]. This is a widely used method to sample random paths from the solution to a master equation derived for Markovian particle systems. Only as the boundary of the

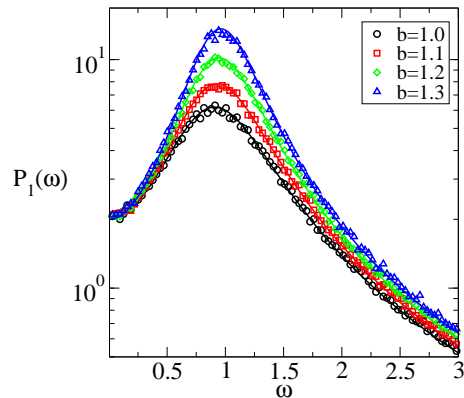


FIG. 2: (Color on-line) Power spectrum $P_1(\omega) = \langle |\tilde{\xi}_1(\omega)|^2 \rangle$ of fluctuations in the concentrations of X_1 molecules in the fixed-point phase ($c = 1, b = 1.8, 1.85, 1.9, 1.95$ from bottom to top at the maximum). Solid lines show results from the analytical theory, markers are from stochastic simulations using Gillespie's algorithm (simulations are run up to $t_f = 150$, system size is $N = 10^5$, averages over 10^4 samples are taken).

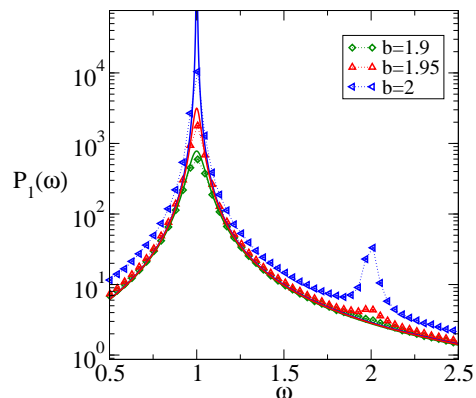


FIG. 3: (Color on-line) Power spectrum $P_1(\omega) = \langle |\tilde{\xi}_1(\omega)|^2 \rangle$ of fluctuations in the concentrations of X_1 molecules in the fixed-point phase near the onset of limit cycle behavior. Solid lines show results from the analytical theory, markers are from stochastic simulations (run up to $t_f = 150$, system size is $N = 10^5$, averages over 10^4 samples are taken).

fixed point phase is approached (i.e. as $b \rightarrow 2$ from below for the fixed value of $c = 1$) do systematic deviations between the theory and Gillespie simulations emerge visibly in Fig. 3. In particular, the power spectra from simulations begin to exhibit peaks at harmonics of the fundamental frequency given by the first maximum, which are not captured by the linear theory. These are the early precursors to the onset of limit cycles due to the stochastic broadening of the Hopf bifurcation. Further discussion of the effect of stochasticity on a Hopf bifurcation can be found in [29].

One of the main points of interest is to see what

happens as the boundary of the fixed point phase is reached. When $b = 1.95$, for example, the peak can be seen to reach a height of 3×10^3 . In fact, it appears from Fig. 3 that as $b \rightarrow 2$ the maximum of $P_1(\omega)$ tends towards infinity. Stochastic effects and resonant amplification of oscillations can hence become macroscopic (i.e. of the same order of magnitude as the mean-field dynamics) for systems of very large system size, close to the transition into limit cycle behavior. This is an extreme case of stochastic amplification due to a resonance as can be seen from Eq. (17): if c is set equal to 1 and $b = 2 - \delta$, the denominator vanishes at frequencies given by $\omega^2 = [1 - (\delta^2/2)] \pm i\delta$. When $b < 2$, there is no zero for real ω , however as $b \rightarrow 2$, the pole approaches the real axis and becomes real at $\omega = 1$ when $b = 2$. The linear stability analysis can be extended into region $b > 2$: for $b = 2 + \tilde{\delta}$, there is an unstable spiral of period 2π . For very small $\tilde{\delta}$, when the exponential growth can be neglected, this is a center of period 2π , which is the nascent limit cycle — not to be confused with a perturbation about the limit cycle to be discussed shortly.

The next section will discuss general technical details of how to characterize the stability of limit cycles in dynamical systems, and we will in particular review elements of Floquet theory and Frenet co-moving frames. Both of these are standard tools used to study dynamical systems exhibiting limit cycles, and are as such not directly concerned with stochastic effects, but with perturbations and fluctuations about periodic attractors in general. We will return to stochastic systems in Section V, before conclusions will be drawn in Section VI.

IV. FLOQUET THEORY AND ROTATION INTO FRENET FRAME

A. Limit cycles in the Brusselator system

In the phases labeled by c) and d) in the phase diagram (Fig. 1), the deterministic Brusselator system, as described by Eq. (1), exhibits limit-cycle behavior since we can eliminate both stable fixed points and unbounded trajectories. For positive initial conditions, Eq. (1) admits a stable periodic solution of period T . The period T will generally depend on the choice of model parameters b and c . It is found that, although T changes significantly with c , if we set $c = 1$ as we do in this paper, and change b only in a narrow band about $b = 2$, the period will change little from the value of 2π found in the last section. Thus in what follows we will find that the angular frequency of the limit cycle remains close to $\omega = 1$.

We will label limit cycle solutions by $\bar{\mathbf{x}}(t) = (\bar{x}_1(t), \bar{x}_2(t))$ in the following calculations and have $\bar{\mathbf{x}}(t + T) = \bar{\mathbf{x}}(t)$ for all times, t . In general the curve,

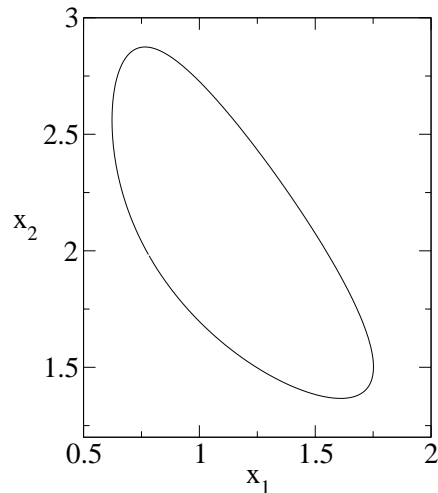


FIG. 4: (Color on-line) Illustration of the limit cycle solution $(\bar{x}_1(t), \bar{x}_2(t))$ of the deterministic Brusselator system at fixed parameters $b = 2.2$, $c = 1$.

$\bar{\mathbf{x}}(t)$, cannot be calculated in closed form. However good estimates can be obtained via numerical integration of Eq. (1). The geometrical shape of the limit cycle of the Brusselator model is illustrated for a fixed choice of the model parameters b and c in Fig. 4.

In order to study stability, we now consider a dynamical path beginning close to, but not on, the limit cycle, $\bar{\mathbf{x}}(t)$. If the limit cycle solution is stable then the difference between this path and the geometric curve of the limit cycle will decay as time progresses. Similarly to the expansion about a fixed point, we can write this difference as

$$\varepsilon \boldsymbol{\xi}(t) = \mathbf{x}(t) - \bar{\mathbf{x}}(t) \quad (18)$$

where, again, ε expresses our anticipation that the deviation from the limit cycle is small. Expanding Eq. (1) in powers of ε and letting $\varepsilon \rightarrow 0$, one then finds that the time evolution of $\boldsymbol{\xi}(t)$ takes on the linear form,

$$\frac{d}{dt} \boldsymbol{\xi}(t) = K(t) \boldsymbol{\xi}(t), \quad (19)$$

where the matrix $K(t)$ is found to take the specific form of Eq. (A-9) for the Brusselator model. Studying the local stability of limit cycle solutions against perturbation is hence the analogue of studying the stability of fixed points as discussed above. The elements of $K(t)$ are given by $K_{ij}(t) = K_{ij}(\bar{\mathbf{x}}(t))$ which is simply the matrix, $K_{ij}(\mathbf{x}) = \partial a_{ij}(\mathbf{x}) / \partial x_j$ evaluated at the limit cycle. Therefore, due to the periodic nature of $\bar{\mathbf{x}}(t)$, all elements of $K(t)$ are periodic.

B. Floquet Theory

An analytical tool to characterize the stability or otherwise of limit cycle solutions is Floquet theory — the mathematical theory of linear differential equations with periodic coefficients (see [30], whose notation we will use). Since, in Eq. (19), we have $K(t+T) = K(t)$, Floquet theory is applicable. In our case, T is the period of the mean-field limit cycle under consideration.

In essence Floquet theory states that, provided $X(t)$ is a fundamental matrix of the system (19), then there exists a non-singular constant matrix B such that

$$X(t+T) = X(t)B \quad (20)$$

for all t . In addition one has

$$\det B = \exp\left(\int_0^T \text{tr}K(t)dt\right). \quad (21)$$

While the matrix B in general depends on the choice of the particular fundamental matrix $X(t)$, its eigenvalues (and determinant) do not. The eigenvalues of B are usually referred to as the Floquet multipliers of the system (19). In the case of the Brusselator the matrices $K(t)$, $X(t)$ and B are 2×2 matrices and we denote the resulting Floquet multipliers by ρ_1 and ρ_2 . Characteristic exponents μ_1 and μ_2 are then defined by setting $\rho_i = e^{\mu_i T}$ for $i \in \{1, 2\}$. Further results of Floquet theory then concern the solutions of (19). If ρ is a characteristic multiplier for (19) and μ the corresponding exponent then it can be shown that there exists a particular solution $\xi(t)$ of (19), such that

$$\xi(t+T) = \rho\xi(t) \quad \forall t. \quad (22)$$

One then finds that this solution can be expressed in terms of a periodic function $\mathbf{p}(t)$ (i.e. one with $\mathbf{p}(t+T) = \mathbf{p}(t)$) scaled by an exponential,

$$\xi(t) = e^{\mu t} \mathbf{p}(t). \quad (23)$$

General solutions of (19) can therefore be written as a linear combination of functions of this form. For example in our two-dimensional system,

$$\xi(t) = c_1 e^{\mu_1 t} \mathbf{p}^{(1)}(t) + c_2 e^{\mu_2 t} \mathbf{p}^{(2)}(t), \quad (24)$$

with c_1, c_2 constant coefficients determined by initial conditions.

The Floquet analysis simplifies for the class of problems where the linear differential equations (19) are derived from a dynamical system, $\dot{\mathbf{x}}(t) = \mathbf{A}(\mathbf{x})$, with a limit cycle $\bar{\mathbf{x}}(t)$. In this case, it is easy to see by differentiation of the original equation of motion that the vector of velocities, $\bar{\mathbf{x}}(t) = (\bar{x}_1(t), \bar{x}_2(t))$, is a solution to (19). Since the velocity vector itself is a periodic function of time, we are therefore assured that one of the Floquet multipliers is equal to

unity, $\rho_1 = 1$. That is, the corresponding exponent, μ_1 , vanishes. This is a general result for all linear expansions about limit cycles arising from first-order equations. The remaining eigenvalue of B can then be determined using Eq. (21) and specifically for the Brusselator system we find that the corresponding Floquet exponent is given by

$$\mu_2 = \frac{1}{T} \int_0^T (-1 - b + 2c\bar{x}_1(t)\bar{x}_2(t) - c\bar{x}_1(t)^2) dt. \quad (25)$$

This integral can be evaluated numerically for any choice of the parameters b, c which give rise to a limit cycle. For $b = 2.2, c = 1$ one finds $\mu_2 = -0.20225$ along with the already established observation that $\mu_1 = 0$. The corresponding functions $\mathbf{p}^{(1)}(t)$ and $\mathbf{p}^{(2)}(t)$ are illustrated in Fig. 5. In fact for the Brusselator the non-zero exponent is bound to be real and negative throughout phases c) and d) of the phase diagram (Fig. 1), i.e. throughout the limit cycle phase.

In conclusion, we have established that one of the Floquet exponents of the system vanishes throughout this phase and that the remaining exponent assumes negative real values. The zero exponent is associated with perturbations in the longitudinal direction of the limit cycle; such perturbations are neither amplified nor reduced as the motion progresses. Perturbations in the transverse direction, by contrast, decay in time in the Brusselator system, rendering the limit cycle stable. Indeed, the multiplier ρ_2 can be seen as characterizing a Poincaré map of transverse motion. If the system is perturbed transversely by a small amount, δ , at time $t = 0$ one may construct a Poincaré map in the usual way [31]: by forming the line perpendicular to the limit cycle which includes the point $\bar{\mathbf{x}}(t = 0)$. Then at every integer multiple nT of the period of the limit cycle the trajectory intersects the line at a distance $\rho_2^n \delta$ from the limit cycle. Since $\rho_2 < 1$, this approaches the limit cycle with increasing n .

C. Rotation into Frenet co-ordinates

As seen above the Floquet exponents and periodic functions of the Brusselator system describe the relaxation of perturbations in longitudinal and transverse directions. It is hence convenient to study the dynamics of deviations in co-ordinates defined along the tangential (longitudinal) and normal (transverse) directions to the limit cycle. This co-moving frame is generally referred to as the Frenet frame [32]. We will label the transverse coordinate by r and the longitudinal one by s , as illustrated in Fig. 6. We follow the procedure of [22] and define $\phi(t)$ to be the angle between the x -axis and the line normal to the limit cycle at time t . Transformation of perturbation displacement vectors from local Cartesian co-ordinates $\xi = (\xi_1, \xi_2)$ into the co-moving Frenet frame $\mathbf{q} \equiv (r, s)$ can then be thought of as a rotation

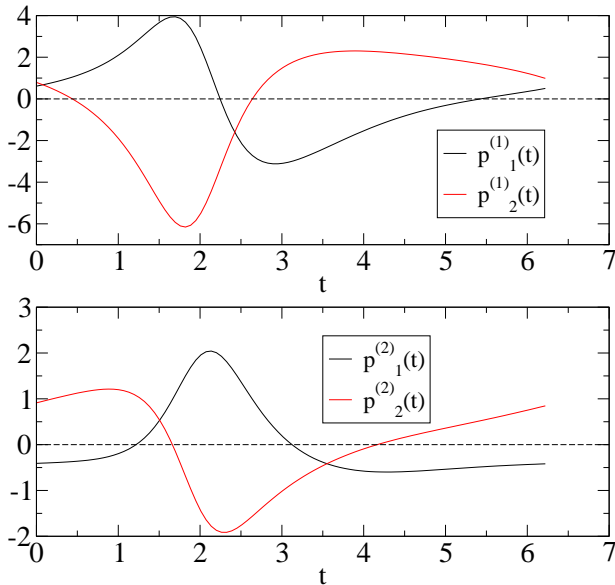


FIG. 5: (Color on-line) Periodic functions of the Floquet analysis of Eq. (19). The curves show each component of the vector-valued functions $\mathbf{p}^{(1)}(t)$ and $\mathbf{p}^{(2)}(t)$ respectively. The function associated with the vanishing exponent is displayed in the upper graph, while that associated with the negative real exponent is displayed in the lower graph.

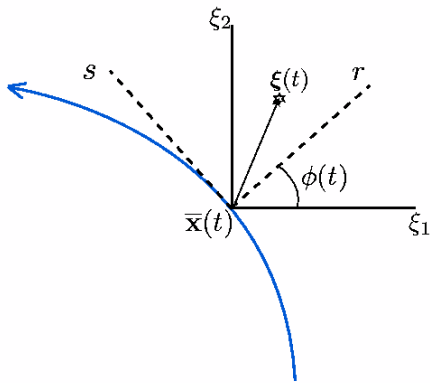


FIG. 6: Illustration of the rotation from Cartesian coordinates (ξ_1, ξ_2) to the Frenet frame, denoted by (r, s) .

by the angle $\phi(t)$, i.e. $\mathbf{q}(t) = J(t)\boldsymbol{\xi}(t)$, where

$$J(t) = \begin{pmatrix} \cos \phi(t) & \sin \phi(t) \\ -\sin \phi(t) & \cos \phi(t) \end{pmatrix}. \quad (26)$$

The angle $\phi(t)$, in turn, can be expressed as a function of the velocity vector $\dot{\bar{\mathbf{x}}}(t)$ at all points on the limit cycle trajectory. The transformation matrix is then

$$J(t) = \frac{1}{v(t)} \begin{pmatrix} \dot{\bar{x}}_2(t) & -\dot{\bar{x}}_1(t) \\ \dot{\bar{x}}_1(t) & \dot{\bar{x}}_2(t) \end{pmatrix}, \quad (27)$$

where $v(t)$ is the speed (magnitude of the velocity) given by $v(t) = \sqrt{(\dot{\bar{x}}_1)^2 + (\dot{\bar{x}}_2)^2}$. The time derivative

of deviations from the limit cycle expressed in the Frenet frame is then given as

$$\begin{aligned} \dot{\mathbf{q}}(t) &= J(t)\dot{\boldsymbol{\xi}}(t) + \dot{J}(t)\boldsymbol{\xi}(t) \\ &= (J(t)K(t)J^{-1}(t) + R(t))\mathbf{q}(t), \end{aligned} \quad (28)$$

where $R(t) = \dot{J}(t)J^{-1}(t)$ has been introduced and explicitly we have,

$$R(t) = \frac{\dot{\bar{x}}_2(t)\ddot{\bar{x}}_1(t) - \dot{\bar{x}}_1(t)\ddot{\bar{x}}_2(t)}{v^2(t)} \begin{pmatrix} 0 & -1 \\ 1 & 0 \end{pmatrix}. \quad (29)$$

To simplify notation we will use $K'(t) \equiv J(t)K(t)J^{-1}(t)$ and $K^{\text{tot}}(t) \equiv K'(t) + R(t)$. As seen in [22] the upper-right element of K^{tot} vanishes identically, i.e. we have $K'_{rs}(t) + R_{rs}(t) = 0$ for all times. Hence, the motion of the first co-ordinate $r(t)$ in the Frenet frame decouples from the second. More precisely, Eq. (19) takes the form

$$\frac{d}{dt} \begin{pmatrix} r(t) \\ s(t) \end{pmatrix} = \begin{pmatrix} K_{rr}^{\text{tot}}(t) & 0 \\ K_{sr}^{\text{tot}}(t) & K_{ss}^{\text{tot}}(t) \end{pmatrix} \begin{pmatrix} r(t) \\ s(t) \end{pmatrix} \quad (30)$$

after rotation into co-moving co-ordinates. The non-trivial elements of K^{tot} can be computed explicitly as functions of the limit cycle trajectory and are given by

$$K_{rr}^{\text{tot}} = \frac{1}{v^2} \left\{ \dot{\bar{x}}_1^2 K_{22} + \dot{\bar{x}}_2^2 K_{11} - \dot{\bar{x}}_1 \dot{\bar{x}}_2 (K_{12} + K_{21}) \right\}, \quad (31)$$

$$K_{sr}^{\text{tot}} = \frac{1}{v^2} \left\{ (\dot{\bar{x}}_2^2 - \dot{\bar{x}}_1^2) (K_{12} + K_{21}) + 2\dot{\bar{x}}_1 \dot{\bar{x}}_2 (K_{11} - K_{22}) \right\}, \quad (32)$$

$$K_{ss}^{\text{tot}} = \dot{v}/v. \quad (33)$$

D. Re-scaled Frenet frame

Further simplification can be achieved by re-scaling the co-ordinates of the Frenet frame, after rotation, by the velocity of the limit cycle. More precisely we make the transformation $\boldsymbol{\chi}(t) \equiv \mathbf{q}(t)/v(t)$, so that

$$\boldsymbol{\chi}(t) = \frac{1}{v(t)} J(t)\boldsymbol{\xi}(t) \equiv \Lambda(t)\boldsymbol{\xi}(t). \quad (34)$$

We will denote the individual components by $\boldsymbol{\chi}(t) = (\rho(t), \sigma(t))$. One finds that the perturbative displacement is described by

$$\dot{\boldsymbol{\chi}}(t) = \left(K^{\text{tot}} - \frac{\dot{v}(t)}{v} I \right) \boldsymbol{\chi}(t) \equiv L^{\text{tot}} \boldsymbol{\chi}(t), \quad (35)$$

where I denotes the identity matrix. Combining Eqs. (30) and (33), Eq. (35) takes the simple form,

$$\frac{d}{dt} \begin{pmatrix} \rho(t) \\ \sigma(t) \end{pmatrix} = \begin{pmatrix} L_{\rho\rho}^{\text{tot}}(t) & 0 \\ L_{\sigma\rho}^{\text{tot}}(t) & 0 \end{pmatrix} \begin{pmatrix} \rho(t) \\ \sigma(t) \end{pmatrix}. \quad (36)$$

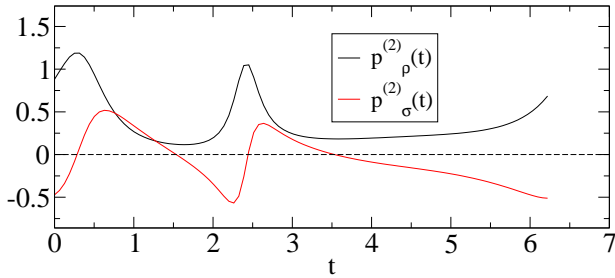


FIG. 7: (Color on-line) Periodic functions $p_\rho^{(2)}(t)$ and $p_\sigma^{(2)}(t)$ associated with the non-trivial Floquet multiplier ρ_2 of Eq. (36). While a perturbation ρ decays in a non-linear fashion, the phase, σ , oscillates.

In particular the lower right element of L^{tot} vanishes identically. The remaining elements are given by

$$L_{\rho\rho}^{\text{tot}}(t) = \frac{1}{v^2} \left\{ (\dot{\bar{x}}_2^2 - \dot{\bar{x}}_1^2)(K_{11} - K_{22}) - 2\dot{\bar{x}}_1\dot{\bar{x}}_2(K_{12} + K_{21}) \right\}, \quad (37)$$

$$L_{\sigma\rho}^{\text{tot}}(t) = \frac{1}{v^2} \left\{ (\dot{\bar{x}}_2^2 - \dot{\bar{x}}_1^2)(K_{12} + K_{21}) + 2\dot{\bar{x}}_1\dot{\bar{x}}_2(K_{11} - K_{22}) \right\}. \quad (38)$$

These relations are valid for general systems of first-order ordinary differential equations with two degrees of freedom which exhibit limit cycle solutions. The vanishing elements in Eq. (36) guarantee the existence of the constant solution $\chi(t) \equiv (0, \sigma_0)$ (with σ_0 a real-valued constant). Hence we find that a perturbation in σ is not only periodic, as indicated by the trivial Floquet exponent, but it is in fact constant. Transverse perturbations relax in a non-trivial way and for completeness we show the associated periodic functions, $p_\rho^{(2)}(t)$ and $p_\sigma^{(2)}(t)$ in Figure 7. The superscript here indicates that we refer to the non-trivial Floquet multiplier ρ_2 . It should be noted that there is a secondary oscillatory effect on σ as ρ decays back to the limit cycle. Since this velocity-scaled rotation yields a simpler linear theory than rotation alone, we will only use the co-ordinates (ρ, σ) in the discussions that follow.

V. STOCHASTIC EFFECTS IN THE LIMIT CYCLE PHASE

A. System size expansion and analytical predictions

We will now return to the stochastic system defined by the chemical reactions (4) or, equivalently, by the master equation (6). In this section we will apply van Kampen's system-size expansion to the case where we have a limit cycle, $(\bar{x}_1(t), \bar{x}_2(t))$, in the mean-field. The starting point is the transformation of random

variables $\mathbf{n} \mapsto \boldsymbol{\xi}(t)$ defined by

$$\mathbf{n} = N\bar{\mathbf{x}}(t) + \sqrt{N}\boldsymbol{\xi}(t). \quad (39)$$

The only difference compared to the transformation (10) we applied in the fixed-point phase is the time dependence of the first term on the right-hand side. Apart from this minor complication the algebraic steps necessary to carry out the expansion of the master equation are mostly unchanged, see the Appendix for details. As before, the evolution of the stochastic fluctuations is described by a linear Langevin equation,

$$\dot{\boldsymbol{\xi}}(t) = K(t)\boldsymbol{\xi} + \mathbf{f}(t), \quad (40)$$

where $\mathbf{f}(t) = (f_1(t), f_2(t))$ is bivariate Gaussian white noise with zero mean with correlations given by, $\langle f_i(t)f_j(t') \rangle = 2D_{ij}(t)\delta(t-t')$ [11, 22]. The forms of the matrices $K(t)$ and $D(t)$ are given in the Appendix (Eqs. (A-9) and (A-10), respectively). Because of the periodicity of $\bar{\mathbf{x}}(t)$, all elements of $K(t)$ and $D(t)$ are periodic with the period of the limit cycle, T .

The linearity of these Langevin equations allows us to make further analytical progress. To this end, it is convenient to study the stochastic dynamics in the velocity-scaled Frenet frame as introduced above. Upon performing a rotation into the co-ordinate system spanned by (ρ, σ) , Eq. (40) takes the form

$$\frac{d}{dt} \begin{pmatrix} \rho(t) \\ \sigma(t) \end{pmatrix} = \begin{pmatrix} L_{\rho\rho}^{\text{tot}}(t) & 0 \\ L_{\sigma\rho}^{\text{tot}}(t) & 0 \end{pmatrix} \begin{pmatrix} \rho(t) \\ \sigma(t) \end{pmatrix} + \begin{pmatrix} \zeta_1(t) \\ \zeta_2(t) \end{pmatrix}, \quad (41)$$

with $\langle \zeta_i(t) \rangle = 0$, $i = 1, 2$ and

$$\langle \zeta_i(t)\zeta_j(t') \rangle = 2[\Lambda(t)D(t)\Lambda^T(t)]_{ij}\delta(t-t'). \quad (42)$$

Hence the correlations of the noise components in the co-moving frame are described by the matrix $H(t) \equiv \Lambda(t)D(t)\Lambda^T(t)$, where $\Lambda(t)$ is defined by Eq. (34).

Since the mean values of both ρ and σ vanish, one can write the variances of these variables as $V_{\rho\rho}(t) = \langle \rho^2(t) \rangle$ and $V_{\sigma\sigma}(t) = \langle \sigma^2(t) \rangle$. First-order ordinary differential equations can be derived [25] for these quantities, and they take the form

$$\dot{V}_{\rho\rho}(t) = 2L_{\rho\rho}^{\text{tot}}V_{\rho\rho}(t) + 2H_{\rho\rho}(t), \quad (43)$$

$$\dot{V}_{\sigma\rho}(t) = L_{\sigma\rho}^{\text{tot}}V_{\rho\rho}(t) + L_{\rho\rho}^{\text{tot}}V_{\sigma\rho}(t) + 2H_{\sigma\rho}(t), \quad (44)$$

$$\dot{V}_{\sigma\sigma}(t) = 2L_{\sigma\rho}^{\text{tot}}V_{\sigma\rho}(t) + 2H_{\sigma\sigma}(t). \quad (45)$$

Solving Eqs (43)-(45) sequentially, a closed form for $V_{\sigma\sigma}(t)$ may be found and evaluated numerically. Results are shown in Fig. 8. Note that the variance of σ , evaluated at integer multiples of the time period, T , increases linearly. This increase without bound means that the linear approximation within which we derived our theoretical results can be expected to be valid only at sufficiently short times. More precisely

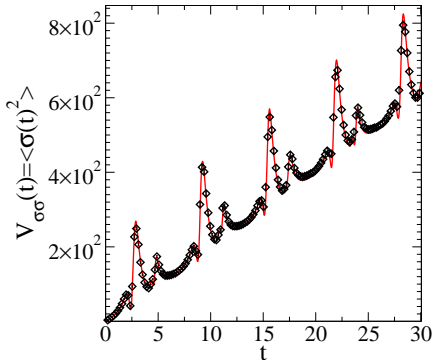


FIG. 8: (Color on-line) Variance $V_{\sigma\sigma}(t)$ of longitudinal fluctuations as obtained from solving Eqs. (43)-(45). Model parameters are fixed to $b = 2.2, c = 1$. The solid line is calculated from the theory while the markers are obtained from simulations. System size is $N = 10^5$, averages over 10000 runs are taken.

the first-order van Kampen expansion is accurate provided $\sigma(t)/\sqrt{N}$ is small compared to the components of the limit cycle solution, $\bar{\mathbf{x}}(t)$. The time scale on which longitudinal fluctuations remain small enough for the linear theory to be valid will hence increase as the system size is increased, and will diverge as $N \rightarrow \infty$.

The Langevin equation for radial fluctuations completely decouples from that of σ . From Eq. (41) we have,

$$\dot{\rho}(t) = L_{\rho\rho}^{\text{tot}}(t)\rho(t) + \zeta_1(t), \quad (46)$$

which is readily integrated, given an initial condition $\rho(t_0) = \rho_0$:

$$\rho(t) - \rho_0\Phi(t, t_0) = \int_{t_0}^t \Phi(t, t')\zeta_1(t')dt', \quad (47)$$

where we have used the definition

$$\Phi(t, t') = \exp\left(\int_{t'}^t L_{\rho\rho}^{\text{tot}}(t'')dt''\right). \quad (48)$$

We can now evaluate the average temporal correlations of radial fluctuations for $\tau > 0$:

$$\begin{aligned} & \langle \rho(t + \tau)\rho(t) \rangle - \rho_0\Phi(t + \tau, t)\Phi^2(t, t_0) \\ &= 2 \int_{t_0}^t \Phi(t + \tau, t')\Phi(t, t')H_{\rho\rho}(t')dt' \\ &= 2\Phi(t + \tau, t) \int_{t_0}^t \Phi^2(t, t')H_{\rho\rho}(t')dt', \end{aligned} \quad (49)$$

where we have used the identity $\phi(t, t')\phi(t', t'') = \phi(t, t'')$, valid for all t, t', t'' . We now set the initialization time to the infinite past ($t_0 \rightarrow -\infty$) so that the initial condition itself is forgotten. After invoking the periodicity of $L_{\rho\rho}(t)$ and $H_{\rho\rho}(t)$ and making

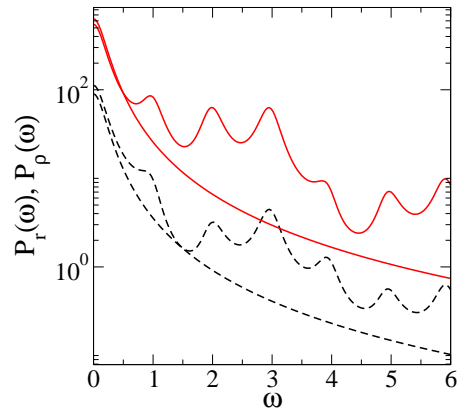


FIG. 9: (Color on-line) Power spectra $P_\rho(\omega)$ and $P_r(\omega)$ of transverse fluctuations in the velocity scaled Frenet frame and ordinary Frenet frame for the Brusselator at $c = 1$ and $b = 2.2$. The solid pair of curves shows results for $P_\rho(\omega)$ while the dashed-line pair shows those without the rescaling of the Frenet frame. The monotonic curves in each case correspond to Lorentzians obtained by replacing $L_{\rho\rho}^{\text{tot}}(t), H_{\rho\rho}(t)$ and $K_{rr}^{\text{tot}}, G_{rr}(t)$ by their time averages in Eq. (50).

a suitable change of the integration variable one finds

$$\begin{aligned} \langle \rho(t + \tau)\rho(t) \rangle &= \frac{2\Phi(t + \tau, t)}{1 - e^{2\mu_\rho}} \\ &\times \int_0^T \Phi^2(t + T, t + t')H_{\rho\rho}(t + t')dt', \end{aligned} \quad (50)$$

where the pre-factor is due to an infinite summation of powers of $e^{2\mu_\rho}$, resulting from the observation that $\Phi(t + T, t) = e^{\mu_\rho}$, where μ_ρ is the non-vanishing Floquet exponent of the system. Eq. (50) confirms that the two-time correlation $\langle \rho(t + \tau)\rho(t) \rangle$ is periodic in t . Averaging over t yields the (time-averaged) auto-correlation function [17, 33],

$$C(\tau) \equiv \frac{1}{T} \int_0^T \langle \rho(t)\rho(t + \tau) \rangle dt. \quad (51)$$

The power spectrum of $\rho(t)$ is now obtained as the inverse Fourier transform of this function $C(\tau)$. A similar procedure can be implemented to compute the power spectrum of $r(t)$, the only necessary replacements being $H_{\rho\rho}(t) \rightarrow G_{rr}(t) \equiv [J(t)D(t)J^T(t)]_{rr}$ and $L_{\rho\rho}^{\text{tot}}(t) \rightarrow K_{rr}^{\text{tot}}(t)$.

The resulting spectra of transverse fluctuations are plotted in Fig. 9, both in the rescaled Frenet frame (the power spectrum is then denoted by $P_\rho(\omega)$), and in the ordinary Frenet frame, see the curve referred to as $P_r(\omega)$. Peaks of a finite width are found at multiples of the frequency of the limit cycle and it can be seen that the structure of these peaks is dependent only on the parameters b and c and not on system size, N . For comparison we also show the

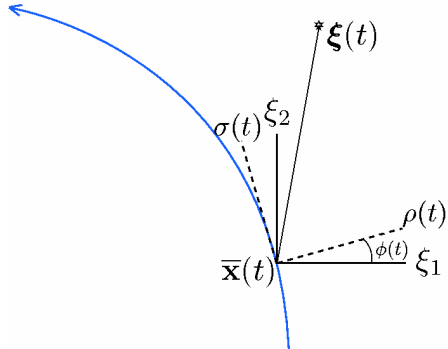


FIG. 10: Illustration of how data is obtained from Gillespie simulations. At any time t the algorithm generates a point $(n_1(t)/N, n_2(t)/N)$ in the x_1, x_2 -plane. The vector components of the vector $\xi(t)$ are then obtained as $\xi_1(t) = N^{1/2} [n_1(t)/N - \bar{x}_1(t)]$ and similarly for $\xi_2(t)$. As before, $\bar{\mathbf{x}}(t)$ is the point marked by the limit cycle trajectory at time t . Subsequently, $\xi(t)$ is converted into co-ordinates $\chi(t) = (\rho(t), \sigma(t))$ by the transformation $\chi(t) = \Lambda(t)\xi(t)$, with $\Lambda(t)$ as defined in Eq. (34).

power spectra one would obtain by replacing the periodic matrices $L^{\text{tot}}(t)$, $K^{\text{tot}}(t)$, $H(t)$ and $G(t)$ by their mean values (e.g. $\bar{H} \equiv T^{-1} \int_0^T H(t) dt$) in Eq. (50). In this case the power spectra reduce to Lorentzian curves which we plot in Fig. 9 along with the full results. It would seem a plausible conclusion that the time-dependence of the drift and diffusion matrices ($L^{\text{tot}}(t)$ and $H(t)$, respectively) contributes additively to the Lorentzian shape that we would expect from a Langevin equation with time-independent drift and diffusion matrices.

B. Test against numerical simulations

The above theoretical prediction for the power spectrum of transverse fluctuations about the mean field behavior can be verified in simulations of *finite* systems using the well known Gillespie algorithm [26] to simulate the reaction system of the Brusselator model. This method generates continuous-time realizations $(n_1(t), n_2(t))$ of the multi-particle stochastic process described by the master equation (6). Note that $n_1(t)$ and $n_2(t)$ are integer valued at all times. The overall system size, N , is a control parameter in these simulations, as are the reactivity parameters b and c .

To make contact with the above theoretical analysis we begin by considering the transformation $\mathbf{n} \mapsto \xi$ given in Eq. (39), i.e. we have,

$$\begin{aligned} n_1(t)/N &= \bar{x}_1(t) + \xi_1(t)/N^{1/2}, \\ n_2(t)/N &= \bar{x}_2(t) + \xi_2(t)/N^{1/2}. \end{aligned} \quad (52)$$

The quantities ρ and σ are then obtained by

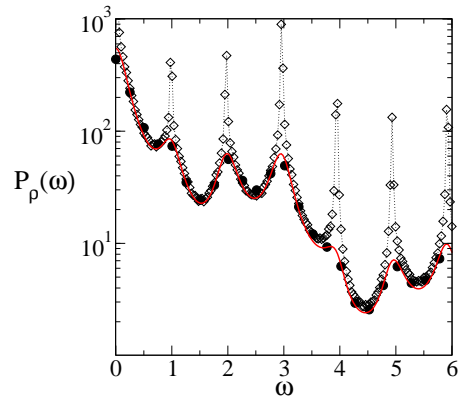


FIG. 11: (Color on-line) Power spectrum $P_\rho(\omega)$ of transverse fluctuations about the limit cycle trajectory. Model parameters are $c = 1, b = 2.2$. The solid curve results from theoretical analysis while filled symbols are from Gillespie simulations run up to $t_f = 25$ and connected open markers are from simulations run up to $t_f = 200$. Simulations interpreted using the rotation method as explained in Section V B. Averages over 10000 samples are taken, system size is $N = 10^5$.

performing the transformation $(\rho(t), \sigma(t))^T = \Lambda(t)(\xi_1(t), \xi_2(t))^T$, with $\Lambda(t)$ as defined in Eq. (34). This is illustrated in Fig. 10.

The linear theory we have developed can be expected to be accurate at most in a regime where the second terms on the right-hand sides of Eq. (52) are both small corrections to the first terms. Equivalently we require that $\rho(t)$ and $\sigma(t)$ both remain small compared to $N^{1/2}$. However, as we have already discussed and demonstrated in Fig. 8, the variance of $\sigma(t)$ grows linearly in time (modulo periodic variations). Hence the results based on the van Kampen expansion are expected to be accurate at most on time scales $t_f = \mathcal{O}(N^0)$. Performing simulations at system size N and run up to time scales $t_f \ll N$ one observes good agreement with the predictions of the linear theory as illustrated by Fig. 11, where we show data for systems of size $N = 10^5$ run up to $t_f = 25$. However, when we consider simulations run up to larger times (e.g. $t_f = 200$), the power spectrum shows systematic deviations from the theoretical curve. This effect can be accounted for by the reasonably steep average slope found in Fig. 8. Extrapolating Fig. 8 to larger times one expects $\langle \sigma(t = 200)^2 \rangle \approx 4000$, i.e. $\left[\langle (\sigma(t = 200)/\sqrt{N})^2 \rangle \right]^{1/2} \approx 0.2$ for $N = 10^5$, so that the second terms on the right-hand sides of Eq. (52) can no longer be thought of as small compared to the first. The next section will discuss an alternative set of measurements that may be taken from Gillespie simulations. These will be shown to successfully tackle this defect and yield a good match with the prediction illustrated in Fig. 9 also on longer time scales.

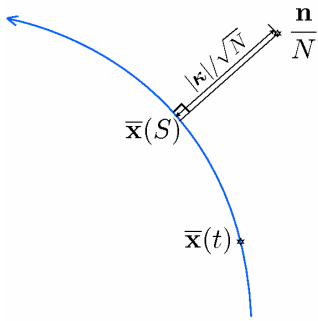


FIG. 12: The modified procedure of identifying deviations from the limit cycle trajectory. The point of reference is now the point on the limit cycle trajectory, which is geometrically closest to the point in the Cartesian plane obtained in Gillespie simulations.

C. Modified method of comparison

The approach that we took in the previous section to interpreting time series from the Gillespie simulations compares extremely well with the theory we have developed in terms of the variance of σ . However, except for simulations performed on very short time scales, we find that this is not the case for the power spectrum of ρ . We will therefore pursue an alternative way of comparing data from Gillespie simulations with the power spectra obtained from the theory. Specifically, the proposal put forward in this section is to use a transformation $\mathbf{n} \mapsto \boldsymbol{\kappa}$ of the form

$$\mathbf{n} = N\bar{\mathbf{x}}(S) + \sqrt{N}\boldsymbol{\kappa}(\mathbf{n}, S), \quad (53)$$

where S is a random variable chosen as

$$S \equiv \arg \min_{t'} |N\bar{\mathbf{x}}(t') - \mathbf{n}|. \quad (54)$$

Here $\arg \min |N\bar{\mathbf{x}}(t') - \mathbf{n}|$ denotes the value t' minimizing the quantity $|N\bar{\mathbf{x}}(t') - \mathbf{n}|$, i.e. S is chosen such that $\bar{\mathbf{x}}(S)$ is the point on the limit cycle trajectory with the minimum distance to the point \mathbf{n}/N obtained from the Gillespie simulation ($|\cdot|$ refers to the Euclidean norm). By construction the vector $\boldsymbol{\kappa}$ is then perpendicular to the velocity of the limit cycle: $\boldsymbol{\kappa}(\mathbf{n}, S) \cdot \dot{\bar{\mathbf{x}}}(S) = 0$. In this way we are able to define a Frenet frame directly in terms of the variable \mathbf{n} which appears in the original master equation, rather than constructing it as a rotation from continuous Cartesian coordinates.

Although our intention is to use this formulation to reinterpret the simulation data, we first have to show how the above construction recovers the results obtained through the van Kampen system-size expansion. Since S is a function of the stochastic variable \mathbf{n} , we may define its mean value as

$$\langle S \rangle_t = \sum_{\mathbf{n}} S(\mathbf{n}) P_{\mathbf{n}}(t), \quad (55)$$

where $P_{\mathbf{n}}(t)$ is the solution of the master equation. Fluctuations about this mean value are defined by

$$S(\mathbf{n}) = \langle S \rangle_t + \frac{1}{\sqrt{N}} \sigma(\mathbf{n}, t). \quad (56)$$

Neglecting terms of order $1/N$, as before, we may Taylor expand about the point $\langle S \rangle_t$ on the curve to obtain

$$\bar{\mathbf{x}}(S) = \bar{\mathbf{x}}(\langle S \rangle_t) + \frac{1}{\sqrt{N}} \sigma(\mathbf{n}, t) \dot{\bar{\mathbf{x}}}(\langle S \rangle_t). \quad (57)$$

Using Eqs. (53) and (57) we have that

$$\mathbf{n} = N\bar{\mathbf{x}}(\langle S \rangle_t) + \sqrt{N} \{ \sigma(\mathbf{n}, t) \dot{\bar{\mathbf{x}}}(\langle S \rangle_t) + \boldsymbol{\kappa}(\mathbf{n}, S) \}. \quad (58)$$

To the order we are working, we may replace \mathbf{n} and S in the curly bracket by $N\bar{\mathbf{x}}(\langle S \rangle_t)$ and $\langle S \rangle_t$ respectively, by using Eqs. (56) and (58). Furthermore from Eq. (58) we have $\mathbf{n} = N\bar{\mathbf{x}}(\langle S \rangle_t)$ to leading order. Since the limit cycle is defined by $\bar{\mathbf{x}}$, the correct mean-field equations are only recovered if the identification $\langle S \rangle_t = t$ is made. These considerations lead to Eq. (58) being written as

$$\mathbf{n} = N\bar{\mathbf{x}}(t) + \sqrt{N} \{ \sigma(t) \dot{\bar{\mathbf{x}}}(t) + \boldsymbol{\kappa}(t) \}. \quad (59)$$

Comparing Eq. (59) with the usual starting point for the van Kampen expansion, Eq. (39), we see that for these two approaches to agree it must be the case that

$$\boldsymbol{\xi}(t) = \sigma(t) \dot{\bar{\mathbf{x}}}(t) + \boldsymbol{\kappa}(t). \quad (60)$$

This is so, since to leading order the condition $\boldsymbol{\kappa}(\mathbf{n}, S) \cdot \dot{\bar{\mathbf{x}}}(S) = 0$ becomes $\boldsymbol{\kappa}(t) \cdot \dot{\bar{\mathbf{x}}}(t) = 0$. Therefore from Eq. (60) we require that $\sigma(t) = \boldsymbol{\xi}(t) \cdot \dot{\bar{\mathbf{x}}}(t) / v^2(t)$. But from $\mathbf{q}(t) = J(t)\boldsymbol{\xi}(t)$ and Eq. (27) it follows that $s(t) = \boldsymbol{\xi}(t) \cdot \dot{\bar{\mathbf{x}}}(t) / v(t)$ and from Eq. (34) that $\sigma(t) = s(t) / v(t)$. This identifies σ as the scaled, longitudinal component introduced in Section IV D. By construction $\boldsymbol{\kappa} = \boldsymbol{\xi} - \sigma \dot{\bar{\mathbf{x}}}$ must be the transverse component. In this way, we recover the van Kampen ansatz used previously.

The Gillespie algorithm generates a time-series for \mathbf{n} which we can use together with knowledge of the equation for the limit cycle to determine S , from Eq. (54). This can then be used (i) to determine σ , which by Eq. (56) and the identification $\langle S \rangle_t = t$ is $\sqrt{N}(S - t)$, (ii) to determine $\boldsymbol{\kappa}$ from Eq. (53), and (iii) to obtain re-scaled transverse fluctuations $\rho(t) = \psi(t) |\boldsymbol{\kappa}(t)| / v(S)$. The function $\psi(t)$ is present to ensure the correct sign; we choose $\psi(t) = -1$ whenever \mathbf{n} is located inside the limit cycle trajectory, and $\psi(t) = 1$ if \mathbf{n} lies outside the area surrounded by the limit cycle. It should be noted that now time is introduced only from the Gillespie algorithm, and not through Eq. (53). Using this methodology, we may determine the power spectra from repeated Gillespie

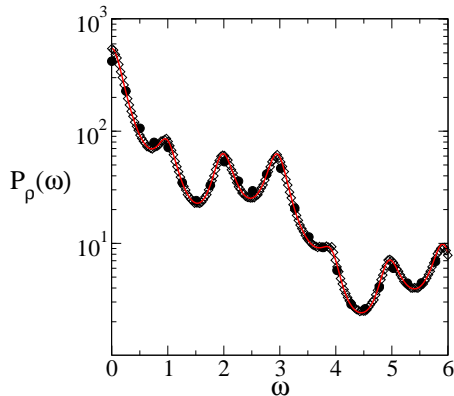


FIG. 13: (Color on-line) Power spectrum $P_\rho(\omega)$ of transverse fluctuations about the limit cycle trajectory. Model parameters are $c = 1, b = 2.2$. The solid curve results from theoretical analysis while filled symbols are from Gillespie simulations run up to $t_f = 25$ and connected open markers are from simulations run up to $t_f = 200$. Simulations are interpreted using the projection method as explained in Section V C. Averages over 10000 samples are taken, system size is $N = 10^5$.

simulations. The results for the variance of σ are indistinguishable from those shown in Figure 8 and so we do not show them. However, in Fig. 13 we compare the power spectrum estimated by measuring $\rho(t) = \psi(t)|\kappa(t)|/v(S)$ from simulations with the analytical results obtained in Section V A (see Eq. (46)). As seen in the figure, we find good quantitative agreement also on time scales on which the method discussed in the previous section failed to reproduce the theoretical curve.

The findings of the section may be summarized by postulating three different temporal regimes. The first regime is defined for times which are sufficiently short that σ/\sqrt{N} can be thought of as small compared with the size of the limit cycle. Thus Eq. (52) may be used, and the modified approach based on Eq. (53) need not be used. The results for $t_f = 25$ exemplify this regime. In the second regime, σ/\sqrt{N} is now sufficiently large that the use of the naive expression (52) leads to a disagreement between simulations and the theoretical curve. This has been discussed above and is exemplified by the results for $t_f = 200$. Finally, at longer times σ will start to probe the periodic structure of the limit cycle, and a different type of behavior will occur. We have not explored this latter regime in the present paper, but we will discuss it again in Section VI.

We end with a further illustration of the difference between the two methods of extracting transverse fluctuations from simulation data. We show an example of a single run in Fig. 14 and depict the resulting two time series $\rho(t)$ produced using the two different methods. Initially the two time series agree well with one another. On longer time scales, how-

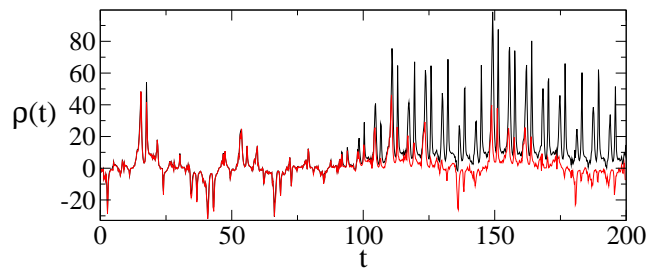


FIG. 14: (Color on-line) Single time series of transverse fluctuations, $\rho(t)$, illustrating the difference between the two measurement methods. The black curve shows data obtained using the rotation method (see Section V B), the red curve shows result from the projection method (see Section V C). Data is obtained from a single Gillespie run at $N = 10^5$ ($b = 2.2, c = 1$).

ever, systematic deviations are observed. We here note that the shape of time series as shown in Fig. 14 can vary considerably between different runs of the stochastic Gillespie simulations. For reasons of clarity the realization shown in the figure is one where the deviation between the time series generated using the two methods is reasonably pronounced at large times. In other runs the discrepancy was smaller.

VI. DISCUSSION

In summary we have carried out an analysis of the effects of internal fluctuations found in finite systems with a large system size, N . We have focused on two-dimensional systems and we have used the Brusselator model as a toy example which we have discussed in two regimes. In the case where the mean-field dynamics approaches a stable fixed-point behavior with complex eigenvalues, we found the expected sustained oscillations driven by the stochasticity of the discrete particle dynamics. The power spectra of these oscillations can be obtained analytically via an expansion in the inverse system-size about the time-independent solution. This is similar to work carried out in the context of other models with fixed-point behavior [2, 7, 8, 10].

One of the aims of the present work was to extend these analytical tools to the case in which the dynamics exhibit a periodic solution on the mean-field level for a range of parameter values. The above van Kampen expansion in the inverse system size can be carried out as before. However, now that we are expanding about a curve, rather than a point, we must make a choice for the point on the limit cycle about which we expand. This scheme may be left undetermined

for carrying out the system-size expansion. However when carrying out simulations, more care has to be exercised when picking the point that one expands about. At short times, the time since the start of the simulation can be used to determine the point along the limit cycle. However, at longer times this will typically not coincide with the nearest point to the quantity \mathbf{n}/N , due to the diffusion in the direction tangential to the limit cycle. We have given a prescription for carrying out simulations in the second temporal regime, and shown how we recover agreement between simulations and the van Kampen expansion using this method. As we pointed out, there is a third regime where σ/\sqrt{N} becomes of the order of the period T , when further modifications will have to be introduced. Eventually, on very long timescales, the diffusive behavior can be studied by using N^{-1} rather than $N^{-1/2}$ as an expansion parameter [25]. It would be interesting to extend the work we have presented here to these longer times.

Another objective was to understand the relation between the cycles due to the stochastic amplification in the fixed point phase and the limit cycles in the phase where the fixed point becomes unstable. We have shown how, for the example of the Brusselator, the former become the latter as one passes through the phase boundary. In the fixed point phase the fluctuations are amplified by a resonance which may be described by a pole in the complex frequency plane. As the phase boundary is approached the pole migrates towards the real axis, reaching it when the boundary is crossed and so turning the resonance into a limit cycle. Although this has been illustrated in the case of the Brusselator, we expect this phenomenon to be generic, and that it may be applied to the various systems mentioned in the Introduction.

The output of the Gillespie algorithm is a time series similar to that which is found in data obtained from real systems. We therefore expect that the methods we have applied in this paper will be applicable to real data. We hope that this will lead to further insights when applied to the many other systems which have a variety of stable attractors and which are subject to intrinsic noise.

Acknowledgments

RPB would like to thank EPSRC for the award of a postgraduate grant. TG is an RCUK Fellow (RCUK reference EP/E500048/1).

APPENDIX: VAN KAMPEN SYSTEM SIZE EXPANSION

In this appendix we briefly sketch some of the mathematical steps involved in carrying out the

system-size expansion for two-dimensional chemical systems, of which the Brusselator is an example. The starting point is the master equation (6),

$$\frac{dP_{\mathbf{n}}(t)}{dt} = \sum_{\nu} (T_{\nu}(\mathbf{n} - \mathbf{v}_{\nu})P_{\mathbf{n}-\mathbf{v}_{\nu}}(t) - T_{\nu}(\mathbf{n})P_{\mathbf{n}}(t)), \quad (\text{A-1})$$

which, subject to an initial condition $P_{\mathbf{n}}(t_0)$, governs the temporal evolution of the probability distribution describing the statistics of the microscopic dynamics as defined by the reactions (4). We determine in Section V that we may use the following mapping between the population vector \mathbf{n} and a continuous fluctuation, $\boldsymbol{\xi}(t)$, about the mean-field concentration as follows,

$$\mathbf{n} = N\mathbf{x}(t) + \sqrt{N}\boldsymbol{\xi}(t). \quad (\text{A-2})$$

Following the procedure of [25] we now formulate the problem in terms the probability distribution $\Pi(\boldsymbol{\xi}, t)$, describing the statistics of the stochastic process $\boldsymbol{\xi}(t)$. Since $\boldsymbol{\xi}(t)$ is a linear transformation of \mathbf{n} we have that $\Pi(\boldsymbol{\xi}, t) \propto P_{\mathbf{n}}(t)$. Hence we may directly substitute $\Pi(\boldsymbol{\xi}, t)$ into the master equation (A-1). We firstly note that the derivative with respect to time in (A-1) is taken at constant \mathbf{n} so that we have $d\boldsymbol{\xi}/dt = -N^{1/2}d\mathbf{x}/dt$. This leads to

$$\begin{aligned} \frac{d\Pi(\boldsymbol{\xi}, t)}{dt} &= \frac{\partial\Pi(\boldsymbol{\xi}, t)}{\partial t} - N^{1/2} \frac{\partial\Pi(\boldsymbol{\xi}, t)}{\partial\xi_1} \frac{dx_1(t)}{dt} \\ &\quad - N^{1/2} \frac{\partial\Pi(\boldsymbol{\xi}, t)}{d\xi_2} \frac{dx_2(t)}{dt}. \end{aligned} \quad (\text{A-3})$$

Next, we write the right-hand side of Eq. (A-1) in terms of $\Pi(\boldsymbol{\xi}, t)$ and find that

$$\begin{aligned} \frac{d\Pi(\boldsymbol{\xi}, t)}{dt} &= \sum_{\nu} \left[\exp(-N^{-1/2}\mathbf{v}_{\nu} \cdot \nabla_{\boldsymbol{\xi}}) - 1 \right] \\ &\quad \times \left[Na_{\nu}(\mathbf{x}(t) + N^{-1/2}\boldsymbol{\kappa})\Pi(\boldsymbol{\xi}, t) \right], \end{aligned} \quad (\text{A-4})$$

where we have also used the re-scaled reaction rates a_{ν} as introduced earlier, i.e.

$$T_{\nu}(N\mathbf{x}(t) + \sqrt{N}\boldsymbol{\xi}) = Na_{\nu} \left(\mathbf{x}(t) + N^{-1/2}\boldsymbol{\xi} \right). \quad (\text{A-5})$$

We have exploited the continuous nature of $\boldsymbol{\xi}$ by using the shift operator: the exponential in the differential operator, $\nabla_{\boldsymbol{\xi}} = \left(\frac{\partial}{\partial\xi_1}, \frac{\partial}{\partial\xi_2} \right)$, used in Eq. (A-4), has the effect of shifting the argument of the subsequent functions by the vector $-N^{-1/2}\mathbf{v}_{\nu}$. Explicitly, for any smooth function, $F(\boldsymbol{\xi})$,

$$\exp(-N^{-1/2}\mathbf{v}_{\nu} \cdot \nabla_{\boldsymbol{\xi}})F(\boldsymbol{\xi}) = F(\boldsymbol{\xi} - N^{-1/2}\mathbf{v}_{\nu}). \quad (\text{A-6})$$

Both the exponential and the rate functions, $a_{\nu}(\mathbf{x})$, in Eq. (A-4) may be expanded as polynomials in $N^{-1/2}$.

We then take the formal limit of $N \rightarrow \infty$ keeping only terms of the two highest orders in N . One may then equate coefficients of powers of N between the left and right-hand sides of the master equation (given by (A-3) and (A-4) respectively).

To leading order one consistently recovers the mean-field equations (7), i.e.

$$\frac{d}{dt}\mathbf{x}(t) = \mathbf{A}(\mathbf{x}(t)), \quad (\text{A-7})$$

with $\mathbf{A}(\mathbf{x}) = \sum_{\nu} \mathbf{v}_{\nu} a_{\nu}(\mathbf{x})$. Expanding to next order one finds

$$\begin{aligned} \frac{\partial}{\partial t}\Pi(\boldsymbol{\xi}, t) = & - \sum_{i,j} K_{ij}(t) \frac{\partial}{\partial \xi_i} (\xi_j \Pi(\boldsymbol{\xi}, t)) \\ & + \sum_{i,j} D_{ij}(t) \frac{\partial}{\partial \xi_i} \frac{\partial}{\partial \xi_j} \Pi(\boldsymbol{\xi}, t), \end{aligned} \quad (\text{A-8})$$

which is a linear Fokker-Planck equation for the distribution $\Pi(\boldsymbol{\xi}, t)$. The elements of the drift matrix $K(t)$ are given by $K_{ij}(t) = \frac{\partial}{\partial x_j} A_i(\mathbf{x}(t))$ and

those in the diffusion matrix $D(t)$ are $D_{ij}(t) = \frac{1}{2} \sum_{\nu} (\mathbf{v}_{\nu})_i (\mathbf{v}_{\nu})_j a_{\nu}(\mathbf{x}(t))$.

For the example of the Brusselator that we use, these matrices are explicitly given by,

$$K(\mathbf{x}) = \begin{pmatrix} -1 - b + 2cx_1x_2 & cx_1^2 \\ b - 2cx_1x_2 & -cx_1^2 \end{pmatrix} \quad (\text{A-9})$$

and

$$D(\mathbf{x}) = \frac{1}{2} \begin{pmatrix} 1 + x_1(1 + b + cx_1x_2) & -x_1(b + cx_1x_2) \\ -x_1(b + cx_1x_2) & x_1(b + cx_1x_2) \end{pmatrix} \quad (\text{A-10})$$

Eq. (A-8) may be considered directly as a stochastic process $\boldsymbol{\xi}(t)$ as described by a Langevin equation. This is discussed in the main text for two cases. In the case of a globally stable fixed point, $\mathbf{x} = \mathbf{x}^*$, $K(\mathbf{x})$ and $D(\mathbf{x})$ become K^* and D^* . In the case of a limit cycle, $\mathbf{x} = \overline{\mathbf{x}}(t)$, the drift and diffusion matrices are functions of time, $K(t)$ and $D(t)$, which naturally pick up the periodicity of this solution.

-
- [1] F. Moss and P. V. E. McClintock, *Noise in Nonlinear Dynamical Systems (3 volumes)* (Cambridge University Press, Cambridge, 1989).
- [2] A. J. McKane and T. J. Newman, *Phys. Rev. Lett.* **94**, 218102 (2005).
- [3] M. Pineda-Krch, H. J. Blok, U. Dieckmann, and M. Doebeli, *Oikos* **116**, 53 (2007).
- [4] J. Cremer, T. Reichenbach, and E. Frey (2008), in press.
- [5] T. Reichenbach, M. Mobilia, and E. Frey, *Phys. Rev. E* **74**, 051907 (2006).
- [6] E. Ben-Naim and P. L. Krapivsky, *Phys. Rev. E* **69**, 046113 (2004).
- [7] M. S. de la Lama, I. G. Szendro, J. R. Iglesias, and H. S. Wio, *Eur. Phys. J. B* **51**, 435 (2006).
- [8] D. Alonso, A. J. McKane, and M. Pascual, *J. R. Soc. Interface* **4**, 575 (2007).
- [9] M. Simoes, M. M. Telo da Gama, and A. Nunes, *J. R. Soc. Interface* **5**, 555 (2008).
- [10] R. Kuske, L. F. Gordillo, and P. Greenwood, *J. Theor. Biol.* **245**, 459 (2007).
- [11] M. Scott, B. Ingalls, and M. Kaern, *Chaos* **16**, 026107 (2006).
- [12] D. Gonze, J. Halloy, and P. Gaspard, *J. Chem. Phys.* **116**, 10997 (2002).
- [13] A. J. McKane, J. D. Nagy, T. J. Newman, and M. O. Stefanini, *J. Stat. Phys.* **128**, 165 (2007).
- [14] M. S. Bartlett, *J. R. Stat. Soc. A* **120**, 48 (1957).
- [15] R. M. Nisbet and W. S. C. Gurney, *Modelling Fluctuating Populations* (Wiley, New York, 1982).
- [16] H. Haken, *Synergetics* (Springer-Verlag, Berlin, 1983).
- [17] C. W. Gardiner, *Handbook of Stochastic Methods* (Springer-Verlag, Berlin, 2004), 3rd ed.
- [18] I. Prigogine and R. Lefever, *J. Chem. Phys.* **48**, 1695 (1968).
- [19] K. J. Brown and F. A. Davidson, *Nonlinear Anal-Theor.* **24**, 1713 (1995).
- [20] P. Gray, S. K. Scott, and J. H. Merkin, *J. Chem. Soc. Farad. T.* **1** **84**, 993 (1988).
- [21] R. Serra, M. Andretta, G. Zanarini, and M. Compiani, *Introduction to the Physics of Complex Systems* (Pergamon Press, Oxford, 1986).
- [22] K. Tomita, T. Ohta, and H. Tomita, *Prog. Theo. Phys.* **52**, 1744 (1974).
- [23] G. Nicolis and I. Prigogine, *Self-Organization in Non-Equilibrium Systems* (Wiley, New York, 1991), 2nd ed.
- [24] A. N. Zaikin and A. M. Zhabotinsky, *Nature* **225**, 535 (1970).
- [25] N. G. van Kampen, *Stochastic Processes in Physics and Chemistry* (Elsevier, Amsterdam, 2007), 3rd ed.
- [26] D. T. Gillespie, *J. Phys. Chem.* **81**, 2340 (1977).
- [27] R. Schraner, S. Grossmann, and P. H. Richter, *Z. Phys. B* **35**, 363 (1979).
- [28] H. Qian, S. Saffarian, and E. L. Elson, *Proc. Natl. Acad. Sci. USA* **99**, 10376 (2002).
- [29] L. L. Arnold, *Random Dynamical Systems* (Springer, Berlin, 2003).
- [30] R. Grimshaw, *Nonlinear Ordinary Differential Equations* (Blackwell, Oxford, 1990).
- [31] S. H. Strogatz, *Nonlinear Dynamics and Chaos* (Perseus Books, Cambridge Mass., 1994).
- [32] C. G. Gibson, *Elementary Geometry of Differentiable Curves* (Cambridge University Press, Cambridge, 2001).
- [33] K. F. Riley, M. P. Hobson, and S. J. Bence, *Mathematical Methods for Physics and Engineering* (Cambridge University Press, Cambridge, 2006), 3rd ed.